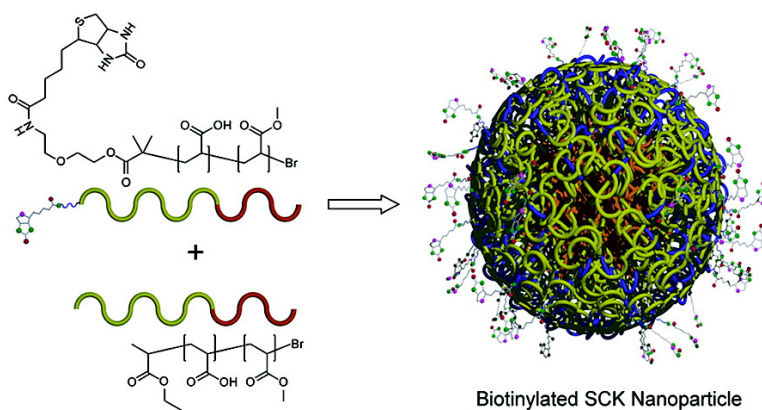Article

Determination of the Bioavailability of Biotin Conjugated onto Shell Cross-Linked (SCK) Nanoparticles

Kai Qi, Qinggao Ma, Edward E. Remsen, Christopher G. Clark,, and Karen L. Wooley

Biotinylated SCK Nanoparticle

More About This Article

Additional resources and features associated with this article are available within the HTML version:

- Supporting Information
- Links to the 16 articles that cite this article, as of the time of this article download
- Access to high resolution figures
- Links to articles and content related to this article
- Copyright permission to reproduce figures and/or text from this article

View the Full Text HTML

ACS Publications
High quality. High impact.

Determination of the Bioavailability of Biotin Conjugated onto Shell Cross-Linked (SCK) Nanoparticles

Kai Qi, Qinggao Ma,[†] Edward E. Remsen,[‡] Christopher G. Clark, Jr.,[§] and
Karen L. Wooley*

*Contribution from the Center for Materials Innovation and Department of Chemistry,
Washington University, One Brookings Drive, Saint Louis, Missouri 63130-4899*

Received November 17, 2003; E-mail: klwooley@artsci.wustl.edu

Abstract: Shell cross-linked nanoparticles (SCKs) presenting surface- and bioavailable biotin functional groups were synthesized via a mixed micelle methodology, whereby co-micellization of chain terminal biotinylated poly(acrylic acid)-*b*-poly(methyl acrylate) (PAA-*b*-PMA) and nonbiotinylated PAA-*b*-PMA were cross-linked in an intramicellar fashion within the shell layer of the mixed micelles, between the carboxylic acid groups of PAA and the amine functionalities of 2,2′-(ethylenedioxy)diethylamine. The hydrodynamic diameters (D_h) of the micelles and the SCKs with different biotinylated block copolymer contents were determined by dynamic light scattering (DLS), and the dimensions of the SCKs were characterized with tapping-mode atomic force microscopy (AFM) and transmission electron microscopy (TEM). The amount of surface-available biotin was tuned by varying the stoichiometric ratio of the biotinylated PAA-*b*-PMA versus the nonbiotinylated PAA-*b*-PMA, as demonstrated with solution-state, binding interaction analyses, an avidin/HABA (avidin/4′-hydroxyazobenzene-2-carboxylic acid) competitive binding assay, and fluorescence correlation spectroscopy (FCS). The avidin/HABA assay found the amount of available biotin at the surface of the biotinylated SCK nanoparticles to increase with increasing biotin-terminated block copolymer incorporation, but to be less than 25% of the theoretical value. FCS measurements showed the same trend.

Introduction

Functionalization of nanoparticles enables tuning of the interactions among themselves as well as with their surrounding environment, by which controlled formation of supramolecular architectures can be achieved.[1-10] These nanostructured materials have potential applications for the construction of devices with unique optical,[11-15] electronic,[16-19] magnetic,[20-22] and catalytic properties.[23-26] Moreover, there has been ever-growing interest in preparing nanoparticles conjugated with biomolecules[27,28] for biomimetics,[29-31] targeted delivery,[32-39] bio-

[†] Present address: New Technology Development Department, Crompton Corp., 400 Elm Street, Building 310, Naugatuck, CT 06770.

[‡] Present address: Cabot Microelectronics Corp., Core Technology Group, 870 North Commons Drive, Aurora, IL 60504.

[§] Present address: Max Planck Institute for Polymer Research, Ackermannweg 10, 55128 Mainz, Germany.

(1) Hamley, I. W. *Angew. Chem., Int. Ed.* **2003**, *42*, 1692−1712.
(2) Cölfen, H.; Mann, S. *Angew. Chem., Int. Ed.* **2003**, *42*, 2350−2365.
(3) Shenhar, R.; Rotello, V. M. *Acc. Chem. Res.* **2003**, *36*, 549−561.
(4) Whitesides, G. M.; Grzybowski, B. *Science* **2002**, *295*, 2418−2421.
(5) Whitesides, G. M.; Boncheva, M. *Proc. Natl. Acad. Sci. U.S.A.* **2002**, *99*, 4769−4774.
(6) Förster, S.; Plantenberg, T. *Angew. Chem., Int. Ed.* **2002**, *41*, 688−714.
(7) Shipway, A. N.; Willner, I. *Chem. Commun.* **2001**, 2035−2045.
(8) Shipway, A. N.; Katz, E.; Willner, I. *ChemPhysChem* **2000**, *1*, 18−52.
(9) Hernandez-Lopez, J. L.; Bauer, R. E.; Chang, W. S.; Glasser, G.; Grebel-Koehler, D.; Klapper, M.; Kreiter, M.; Leclaire, J.; Majoral, J. P.; Mittler, S.; Müllen, K.; Vasilev, K.; Weil, T.; Wu, J.; Zhu, T.; Knoll, W. *Mater. Sci. Eng., C* **2003**, *C23*, 267−274.
(10) Storhoff, J. J.; Mirkin, C. A. *Chem. Rev.* **1999**, *99*, 1849−1862.
(11) Gerion, D.; Pinaud, F.; Williams, S. C.; Parak, W. J.; Zanchet, D.; Weiss, S.; Alivisatos, A. P. *J. Phys. Chem. B* **2001**, *105*, 8861−8871.
(12) Mattoussi, H.; Mauro, J. M.; Goldman, E. R.; Green, T. M.; Anderson, G. P.; Sundar, V. C.; Bawendi, M. G. *Phys. Status Solidi B* **2001**, *224*, 277−283.
(13) Murray, C. B.; Kagan, C. R.; Bawendi, M. G. *Annu. Rev. Mater. Sci.* **2000**, *30*, 545−610.
(14) Elghanian, R.; Storhoff, J. J.; Mucic, R. C.; Letsinger, R. L.; Mirkin, C. A. *Science* **1997**, *277*, 1078−1080.
(15) Holtz, J. H.; Asher, S. A. *Nature* **1997**, *389*, 829−832.
(16) Milliron, D. J.; Alivisatos, A. P.; Pitois, C.; Edder, C.; Fréchet, J. M. J. *Adv. Mater.* **2003**, *15*, 58−61.
(17) Coe, S.; Woo, W.-K.; Bawendi, M.; Bulović, V. *Nature* **2002**, *420*, 800−803.
(18) Park, S.-J.; Lazarides, A. A.; Mirkin, C. A.; Brazis, P. W.; Kannewurf, C. R.; Letsinger, R. L. *Angew. Chem., Int. Ed.* **2000**, *39*, 3845−3848.
(19) Anicet, N.; Bourdillon, C.; Moiroux, J.; Savéant, J.-M. *J. Phys. Chem. B* **1998**, *102*, 9844−9849.
(20) Wang, X.-S.; Arsenault, A.; Ozin, G. A.; Winnik, M. A.; Manners, I. *J. Am. Chem. Soc.* **2003**, *125*, 12686−12687.
(21) Ginzburg, M.; MacLachlan, M. J.; Yang, S. M.; Coombs, N.; Coyle, T. W.; Raju, N. P.; Greedan, J. E.; Herber, R. H.; Ozin, G. A.; Manners, I. *J. Am. Chem. Soc.* **2002**, *124*, 2625−2639.
(22) Yan, X.; Liu, G.; Liu, F.; Tang, B. Z.; Peng, H.; Pakhomov, A. B.; Wong, C. Y. *Angew. Chem., Int. Ed.* **2001**, *40*, 3593−3596.
(23) Bosman, A. W.; Vestberg, R.; Heumann, A.; Fréchet, J. M. J.; Hawker, C. J. *J. Am. Chem. Soc.* **2003**, *125*, 715−728.
(24) Hecht, S.; Fréchet, J. M. J. *Angew. Chem., Int. Ed.* **2001**, *40*, 74−91.
(25) Piotti, M. E.; Rivera, F., Jr.; Bond, R.; Hawker, C. J.; Fréchet, J. M. J. *J. Am. Chem. Soc.* **1999**, *121*, 9471−9472.
(26) Klingelhöfer, S.; Heitz, W.; Greiner, A.; Oestreich, S.; Förster, S.; Antonietti, M. *J. Am. Chem. Soc.* **1997**, *119*, 10116−10120.
(27) Niemeyer, C. M. *Angew. Chem., Int. Ed.* **2001**, *40*, 4128−4158.
(28) Narain, R.; Armes, S. P. *Macromolecules* **2003**, *36*, 4675−4678.
(29) Sarikaya, M.; Tamerler, C.; Jen, A. K. Y.; Schulten, K.; Baneyx, F. *Nat. Mater.* **2003**, *2*, 577−585.
(30) Thibault, R. J., Jr.; Galow, T. H.; Turnberg, E. J.; Gray, M.; Hotchkiss, P. J.; Rotello, V. M. *J. Am. Chem. Soc.* **2002**, *124*, 15249−15254.
(31) Mann, S. *Angew. Chem., Int. Ed.* **2000**, *39*, 3392−3406.
(32) Choi, S.-W.; Kim, W.-S.; Kim, J.-H. *J. Dispersion Sci. Technol.* **2003**, *24*, 475−487.
(33) Berry, C. C.; Curtis, A. S. G. *J. Phys. D: Appl. Phys.* **2003**, *36*, R198−R206.
(34) Kakizawa, Y.; Kataoka, K. *Adv. Drug Delivery Rev.* **2002**, *54*, 203−222.

detection,[40−44] diagnosis, and treatment purposes,[33,45−49] each of which depends on the biomolecule nanoparticle conjugates remaining bioactive and bioavailable after conjugation.

Shell cross-linked nanoparticles (SCKs),[50−58] a class of well-defined, polymeric, nanostructured materials with a hydrophobic core domain and a hydrophilic shell layer, have received recent attention as biocompatible[59] and stable[60] nanoscale scaffolds from which bioactive elements can be presented.[61−64] The general methodology that has been developed for the preparation of SCKs involves the supramolecular assembly of block copolymers into polymer micelles,[65−68] followed by covalent cross-linking reactions throughout the shell layer. Synthetic strategies for surface functionalization of SCKs have also been established,[69] based upon mixed micelle formation[70,71] or postpreparation functionalization reactions.[64] In each case, the determination of the surface- and bioavailability of the functional groups covalently linked within the hydrogel-like shell layer of 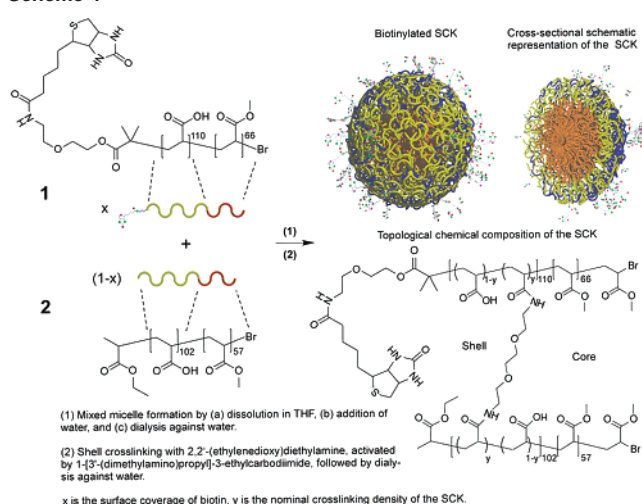the SCKs remains challenging, due to the interplay of the confinement versus flexibility of the partially crosslinked polymer chains constituting the SCK shell,[72,73] the mobility of the entire nanostructure,[74,75] and the composition of the functional groups.

The interaction of biotin and avidin as a ligand−receptor pair, widely used in the field of biology and medicine for purification, localization, and diagnostics, has served as a well-defined model system to probe bioavailability.[76,77] Applications utilizing protein recognition of biotinylated species, including small molecules, polymers, lipids, nucleic acids, proteins, and nanoparticles, have been extended to fabricate novel nanoscopic assemblies, such as two-dimensional arrays of biotin−avidin conjugates,[78] protein−polymer amphiphiles,[79] protein−lipid monolayers,[80] protein multilayers,[81] protein−polymer multilayers,[82] protein−DNA multilayers,[19,83] protein−nanoparticle composites,[84−87] and functionalized surfaces,[88−92] among others. Biotinylated nanoparticles,[93−95] and microparticles[96,97] with sizes ranging from globular proteins to cells, have been utilized as model systems to study and mimic the multivalent interactions[30,98−100] that occur in protein−cell recognition and cell−cell adhesion processes.[96,101]

Given the high application potential and fundamental significance of biotinylated nanoparticles, the synthesis and study of biotinylated SCKs were undertaken. Interest in these materials

(35) Kataoka, K.; Harada, A.; Nagasaki, Y. *Adv. Drug Delivery Rev.* **2001**, *47*, 113−131.
(36) Langer, R. *Science* **2001**, *293*, 58−59.
(37) Lynn, D. M.; Amiji, M. M.; Langer, R. *Angew. Chem., Int. Ed.* **2001**, *40*, 1707−1710.
(38) Langer, R. *Nature* **1998**, *392*, 5−10.
(39) Savić, R.; Luo, L.; Eisenberg, A.; Maysinger, D. *Science* **2003**, *300*, 615−618.
(40) Nam, J.-M.; Thaxton, C. S.; Mirkin, C. A. *Science* **2003**, *301*, 1884−1886.
(41) Cao, Y. C.; Jin, R.; Mirkin, C. A. *Science* **2002**, *297*, 1536−1540.
(42) Taton, T. A.; Mirkin, C. A.; Letsinger, R. L. *Science* **2000**, *289*, 1757−1760.
(43) Willner, I.; Shipway, A. N.; Willner, B. *ACS Symp. Ser.* **2003**, *844*, 88−105.
(44) Velev, O. D.; Kaler, E. W. *Langmuir* **1999**, *15*, 3693−3698.
(45) Pankhurst, Q. A.; Connolly, J.; Jones, S. K.; Dobson, J. *J. Phys. D: Appl. Phys.* **2003**, *36*, R167−R181.
(46) Hamblett, K. J.; Kegley, B. B.; Hamlin, D. K.; Chyan, M.-K.; Hyre, D. E.; Press, O. W.; Wilbur, D. S.; Stayton, P. S. *Bioconjugate Chem.* **2002**, *13*, 588−598.
(47) Alivisatos, A. P. *Sci. Am.* **2001**, *285*, 67−73.
(48) Wilbur, D. S.; Pathare, P. M.; Hamlin, D. K.; Weerawarna, S. A. *Bioconjugate Chem.* **1997**, *8*, 819−832.
(49) Wilbur, S. D.; Hamlin, D. K.; Vessella, R. L.; Stray, J. E.; Buhler, K. R.; Stayton, P. S.; Klumb, L. A.; Pathare, P. M.; Weerawarna, S. A. *Bioconjugate Chem.* **1996**, *7*, 689−702.
(50) Wooley, K. L. *J. Polym. Sci., Part A: Polym. Chem.* **2000**, *38*, 1397−1407.
(51) Wooley, K. L. *Chem.−Eur. J.* **1997**, *3*, 1397−1399.
(52) Thurmond, K. B., II; Kowalewski, T.; Wooley, K. L. *J. Am. Chem. Soc.* **1996**, *118*, 7239−7240.
(53) Thurmond, K. B., II; Kowalewski, T.; Wooley, K. L. *J. Am. Chem. Soc.* **1997**, *119*, 6656−6665.
(54) Huang, H.; Wooley, K. L.; Remsen, E. E. *Chem. Commun.* **1998**, 1415−1416.
(55) Ding, J.; Liu, G. *Macromolecules* **1998**, *31*, 6554−6558.
(56) Bütün, V.; Billingham, N. C.; Armes, S. P. *J. Am. Chem. Soc.* **1998**, *120*, 12135−12136.
(57) Sanji, T.; Nakatsuka, Y.; Kitayama, F.; Sakurai, H. *Chem. Commun.* **1999**, 2201−2202.
(58) Cao, L.; Manners, I.; Winnik, M. A. *Macromolecules* **2001**, *34*, 3353−3360.
(59) Becker, M. L.; Joralemon, M. J.; Remsen, E. E.; Endres, P. J.; Cegelski, L.; Huang, H.; Schaefer, J.; Wooley, K. L. *Polym. Prepr.* **2002**, *43*, 682−683.
(60) Clark, C. G., Jr.; Wooley, K. L. *Curr. Opin. Colloid Interface Sci.* **1999**, *4*, 122−129.
(61) Thurmond, K. B., II; Remsen, E. E.; Kowalewski, T.; Wooley, K. L. *Nucleic Acids Res.* **1999**, *27*, 2966.
(62) Liu, J.; Zhang, Q.; Remsen, E. E.; Wooley, K. L. *Biomacromolecules* **2001**, *2*, 362−368.
(63) Becker, M. L.; Liu, J.; Wooley, K. L. *Chem. Commun.* **2003**, 802−803.
(64) Pan, D.; Turner, J. L.; Wooley, K. L. *Chem. Commun.* **2003**, 2400−2401.
(65) Discher, D. E.; Eisenberg, A. *Science* **2002**, *297*, 967−973.
(66) Zhang, L.; Eisenberg, A. *Science* **1995**, *268*, 1728−1731.
(67) Zhang, L.; Yu, K.; Eisenberg, A. *Science* **1996**, *272*, 1777−1779.
(68) Matějíček, P.; Uhlík, F.; Limpouchová, Z.; Procházka, K.; Tuzar, Z.; Webber, S. E. *Macromolecules* **2002**, *35*, 9487−9496.
(69) Becker, M. L.; Joralemon, M. J.; Liu, J.; Ma, Q.; Murthy, K. S.; Qi, K.; Remsen, E. E.; Zhang, Q.; Wooley, K. L. *Polym. Prepr.* **2002**, *43*, 323.
(70) Matějíček, P.; Humpolíčková, J.; Procházka, K.; Tuzar, Z.; Špírková, M.; Hof, M.; Webber, S. E. *J. Phys. Chem. B* **2003**, *107*, 8232−8240.
(71) Terreau, O.; Luo, L.; Eisenberg, A. *Langmuir* **2003**, *19*, 5601−5607.

(72) Huang, H.; Wooley, K. L.; Schaefer, J. *Macromolecules* **2001**, *34*, 547−551.
(73) O'Connor, R. D.; Zhang, Q.; Wooley, K. L.; Schaefer, J. *Helv. Chim. Acta* **2002**, *85*, 3219−3224.
(74) Huang, H.; Kowalewski, T.; Wooley, K. L. *J. Polym. Sci., Part A* **2003**, *41*, 1659−1668.
(75) Murthy, K. S.; Ma, Q.; Remsen, E. E.; Kowalewski, T.; Wooley, K. L. *J. Mater. Chem.* **2003**, *13*, 2785−2795.
(76) Wilchek, M.; Bayer, E. A. *Anal. Biochem.* **1988**, *171*, 1−32.
(77) Wilchek, M.; Bayer, E. A. *Methods Enzymol.* **1990**, *184*, 5−13.
(78) Wang, S.-W.; Robertson, C. R.; Gast, A. P. *Langmuir* **1999**, *15*, 1541−1548.
(79) Hannink, J. M.; Cornelissen, J. J. L. M.; Farrera, J. A.; Foubert, P.; De Schryver, F. C.; Sommerdijk, N. A. J. M.; Nolte, R. J. M. *Angew. Chem., Int. Ed.* **2001**, *40*, 4732−4734.
(80) Ahlers, M.; Mueller, W.; Reichert, A.; Ringsdorf, H.; Venzmer, J. *Angew. Chem.* **1990**, *102*, 1310−1327.
(81) Müller, W.; Ringsdorf, H.; Rump, E.; Wildburg, G.; Zhang, X.; Angermaier, L.; Knoll, W.; Liley, M.; Spinke, J. *Science* **1993**, *262*, 1706−1708.
(82) Anzai, J.-i.; Nishimura, M. *J. Chem. Soc., Perkin Trans. 2* **1997**, 1887−1889.
(83) Ijiro, K.; Ringsdorf, H.; Birch-Hirschfeld, E.; Hoffmann, S.; Schilken, U.; Strube, M. *Langmuir* **1998**, *14*, 2796−2800.
(84) Park, S.-J.; Lazarides, A. A.; Mirkin, C. A.; Letsinger, R. L. *Angew. Chem., Int. Ed.* **2001**, *40*, 2909−2912.
(85) Lala, N.; Sastry, M. *Phys. Chem. Chem. Phys.* **2000**, *2*, 2461−2466.
(86) Mann, S.; Shenton, W.; Li, M.; Connolly, S.; Fitzmaurice, D. *Adv. Mater.* **2000**, *12*, 147−150.
(87) Shenton, W.; Davis, S. A.; Mann, S. *Adv. Mater.* **1999**, *11*, 449−452.
(88) Faucher, K. M.; Sun, X.-L.; Chaikof, E. L. *Langmuir* **2003**, *19*, 1664−1670.
(89) Sun, X.-L.; Faucher, K. M.; Houston, M.; Grande, D.; Chaikof, E. L. *J. Am. Chem. Soc.* **2002**, *124*, 7258−7259.
(90) Lahann, J.; Balcells, M.; Rodon, T.; Lee, J.; Choi, I. S.; Jensen, K. F.; Langer, R. *Langmuir* **2002**, *18*, 3632−3638.
(91) Hyun, J.; Zhu, Y.; Liebmann-Vinson, A.; Beebe, T. P., Jr.; Chilkoti, A. *Langmuir* **2001**, *17*, 6358−6367.
(92) Hyun, J.; Chilkoti, A. *J. Am. Chem. Soc.* **2001**, *123*, 6943−6944.
(93) Gref, R.; Couvreur, P.; Barratt, G.; Mysiakine, E. *Biomaterials* **2003**, *24*, 4529−4537.
(94) Schroedter, A.; Weller, H. *Angew. Chem., Int. Ed.* **2002**, *41*, 3218−3221.
(95) Sastry, M.; Lala, N.; Patil, V.; Chavan, S. P.; Chittiboyina, A. G. *Langmuir* **1998**, *14*, 4138−4142.
(96) Cannizzaro, S. M.; Padera, R. F.; Langer, R.; Rogers, R. A.; Black, F. E.; Davies, M. C.; Tendler, S. J. B.; Shakesheff, K. M. *Biotechnol. Bioeng.* **1998**, *58*, 529−535.
(97) Gao, J.; Niklason, L.; Zhao, X.-M.; Langer, R. *J. Pharm. Sci.* **1998**, *87*, 246−248.
(98) Mammen, M.; Chio, S.-K.; Whitesides, G. M. *Angew. Chem., Int. Ed.* **1998**, *37*, 2755−2794.
(99) Cairo, C. W.; Gestwicki, J. E.; Kanai, M.; Kiessling, L. L. *J. Am. Chem. Soc.* **2002**, *124*, 1615−1619.
(100) Boal, A. K.; Rotello, V. M. *J. Am. Chem. Soc.* **2000**, *122*, 734−735.
(101) Barrientos, A. G.; de la Fuente, J. M.; Rojas, T. C.; Fernández, A.; Penadés, S. *Chem.-Eur. J.* **2003**, *9*, 1909−1921.

Scheme 1

(1) Mixed micelle formation by (a) dissolution in THF, (b) addition of water, and (c) dialysis against water.

(2) Shell crosslinking with 2,2'-(ethylenedioxy)diethylamine, activated by 1-[3'-(dimethylamino)propyl]-3-ethylcarbodiimide, followed by dialysis against water.

x is the surface coverage of biotin, y is the nominal crosslinking density of the SCK.

Figure 1. ¹H NMR spectra of (a) biotin, **4**, (b) biotinylated alcohol, **5**, and (c) biotinylated initiator, **3**, in CD₃OD.

Scheme 2

is based primarily upon their value in the determination of the surface- and bioavailability of functional groups that are incorporated into the SCK nanostructure via a mixed micelle methodology. The mixed micelle methodology, nominally, is a co-micellization process involving amphiphilic block copolymers, at least one of which contains a biotin unit as the hydrophilic chain terminus. It is expected that an advantage of the mixed micelle strategy is the ability to control the degree of surface coverage by the biotin functional groups, via control over the stoichiometric ratio of the chain end functionalized and nonfunctionalized, amphiphilic block copolymers. Although the placement of the functionality is at the hydrophilic chain end, the actual location of this functionality with respect to the SCK's surface will depend on many factors. These include conformations of the polymer chains, which are dependent upon the nature of the chain end functionality, the composition of the block copolymers, the conditions employed for micelle formation, and the reaction conditions during shell cross-linking.[102−104] It was hypothesized that at least a portion of the functional groups, which are biotin in this particular case, will be surface-exposed after both micellization and shell cross-linking. The results of the present study support this hypothesis based on detailed solution-state, binding interaction analyses, employing an avidin/HABA (avidin/4′-hydroxyazobenzene-2-carboxylic acid) competitive binding assay and fluorescence correlation spectroscopy (FCS).

Results and Discussion

The preparation of biotinylated SCK nanoparticles via the mixed micelle methodology involves a combination of co-micellization and covalent stabilization within the shell layer (Scheme 1). The block copolymer precursors were designed to be composed of similar hydrophobic and hydrophilic block segment compositions and lengths to provide a uniform distribution of the mixed polymer chains throughout the micelles.[105,106]

In addition, the hydrophilic block segment that carried the biotin unit was lengthened to enhance its presentation on the surfaces of the micelles and the corresponding SCKs. To further increase the solubility of the biotin functional group in aqueous media and to reduce interparticle aggregation, which could potentially result from the functionalized chain end, an ethylene oxide linker was used.[107] Therefore, amphiphilic diblock copolymers, poly-(acrylic acid)-*b*-poly(methyl acrylate) (PAA-*b*-PMA) with, **1**, and without, **2**, a biotin chain terminus, were prepared for co-micellization, followed by intramicellar cross-linking. Nano-structures were prepared using 0%, 0.2%, 1%, 2%, 10%, 40%, and 100% biotinylated block copolymer. These ratios were selected to span from low numbers of biotin to full biotinylation.

The synthesis of block copolymer, **1**, having a biotin unit at the hydrophilic chain terminus, utilized a biotinylated initiator, **3**, for atom transfer radical polymerization (ATRP) (Scheme 2). Biotin, **4**, was first activated by 1,1′-carbonyldiimidazole, followed by coupling to a hydrophilic linker 2-(2′-aminoethoxy)-ethanol to form the biotinylated alcohol, **5**. Esterification of **5** with 2-bromo-2-methyl propionic acid, mediated by 4-(*N,N*-dimethylamino)pyridine (DMAP) and 1,3-dicyclohexylcarbodiimide (DCC), afforded **3** in 43% yield after purification by flash chromatography. The composite of ¹H NMR spectra (Figure 1) indicates the formation of **3**, wherein the methylene resonance for the protons labeled as H_j of **5** shifted downfield to 4.2 ppm, overlapping with the protons H_e and H_f on the biotin unit, upon formation of **3**. The appearance of the singlet resonating at 1.9 ppm confirmed the presence of the isobutyryl methyl groups of **3**. The urea protons on biotin were not observed, due to the rapid proton exchange with the solvent, CD₃OD.

Preparation of the block copolymers, **9** and **10**, was accomplished by sequential ATRP of *tert*-butyl acrylate and methyl acrylate, initiated from **3** and **6**, respectively (Scheme

(102) Ma, Q.; Remsen, E. E.; Clark, C. G., Jr.; Kowalewski, T.; Wooley, K. L. *Proc. Natl. Acad. Sci. U.S.A.* **2002**, *99*, 5058−5063.
(103) Ma, Q.; Remsen, E. E.; Kowalewski, T.; Wooley, K. L. *J. Am. Chem. Soc.* **2001**, *123*, 4627−4628.
(104) Huang, H.; Kowalewski, T.; Remsen, E. E.; Gertzmann, R.; Wooley, K. L. *J. Am. Chem. Soc.* **1997**, *119*, 11653−11659.
(105) Tian, M.; Qin, A.; Ramireddy, C.; Webber, S. E.; Munk, P.; Tuzar, Z.; Procházka, K. *Langmuir* **1993**, *9*, 1741−1748.
(106) Qin, A.; Tian, M.; Ramireddy, C.; Webber, S. E.; Munk, P.; Tuzar, Z. *Macromolecules* **1994**, *27*, 120−126.
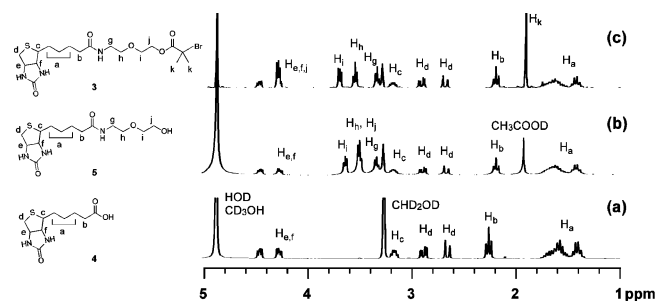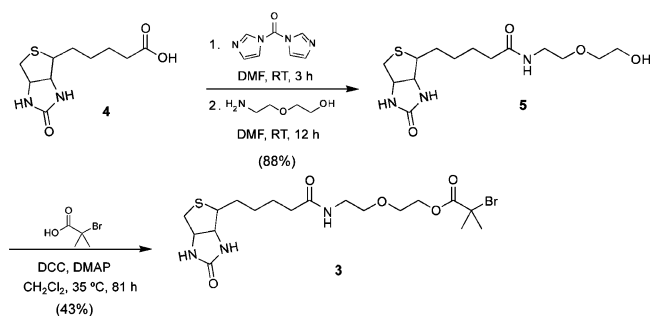(107) Bütün, V.; Wang, X. S.; de Paz Báñez, M. V.; Robinson, K. L.; Billingham, N. C.; Armes, S. P.; Tuzar, Z. *Macromolecules* **2000**, *33*, 1−3.
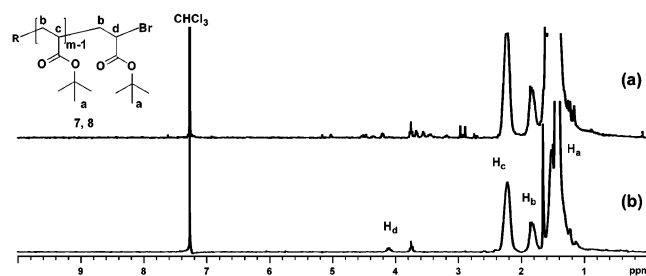
Figure 2. ^{1}H NMR spectra of (a) biotinylated P*t*BA, **7**, and (b) nonbiotinylated P*t*BA, **8**, in CDCl₃.
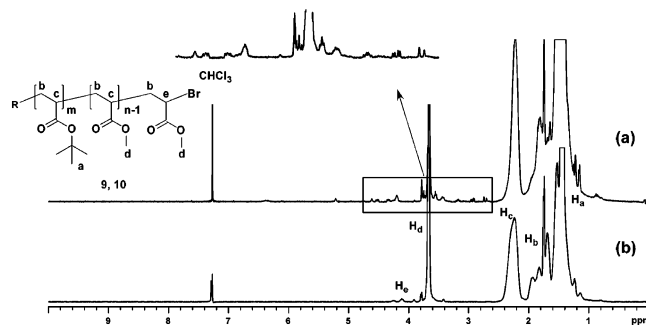

Figure 3. ^{1}H NMR of spectra (a) biotinylated P*t*BA-*b*-PMA, **9**, and (b) nonbiotinylated P*t*BA-*b*-PMA, **10**, in CDCl₃. A magnified view of proton resonances from the biotin unit is also shown.

3). Polymerization of *tert*-butyl acrylate initiated by **3**, using CuBr/*N*,*N*,*N*′,*N*″,*N*″-pentamethyldiethylenetriamine (PMDETA) as the catalyst/ligand system, was allowed to proceed at 55 °C to 76% conversion to give a 56% yield of biotinylated poly-(*tert*-butyl acrylate) (P*t*BA) homopolymer, **7**. A small amount of *N*,*N*-dimethylformamide was added to solvate **3** and provide for a homogeneous polymerization mixture. Growth of the methyl acrylate chain segment from **7** was performed in bulk, in the presence of CuBr/PMDETA at 50 °C, and was allowed to proceed to <10% conversion, giving biotinylated poly(*tert*-butyl acrylate)-*b*-poly(methyl acrylate) (P*t*BA-*b*-PMA) diblock copolymer, **9**, in 41% yield. The synthesis of the nonbiotinylated P*t*BA homopolymer, **8**, and the corresponding P*t*BA-*b*-PMA diblock copolymer, **10**, followed a similar route, using ethyl 2-bromopropionate, **6**, as the ATRP initiator. The presence of the biotin functional group at the chain terminus was confirmed by ^{1}H NMR spectroscopy for the biotinylated homopolymer, **7**, and the biotinylated diblock copolymer, **9**, which are shown in Figures 2 and 3, in comparison to their nonbiotinylated analogues **8** and **10**, respectively. In Figure 3, a magnified view of a region of the ^{1}H NMR spectrum for the biotinylated diblock copolymer is provided to illustrate the resonances for H_c, H_d, H_e, and H_f of the biotin unit. The molecular weights and molecular weight distributions of polymers, **7**–**10**, were determined by size exclusion chromatography (SEC), equipped with multiangle laser light scattering and refractive index detection. The molecular weights were also determined via ^{1}H NMR end group analysis. The results are summarized in Table 1.

The *tert*-butyl ester groups on **9** and **10** were cleaved selectively by reaction with trifluoroacetic acid (TFA) in dichloromethane for ca. 14 h at room temperature. After removal of the solvent and excess TFA, the residue was dissolved in THF, and the amphiphilic block copolymers were purified by dialysis against deionized water (cellulose membrane dialysis tubing, MWCO 6000–8000 Da). Isolation of the amphiphilic
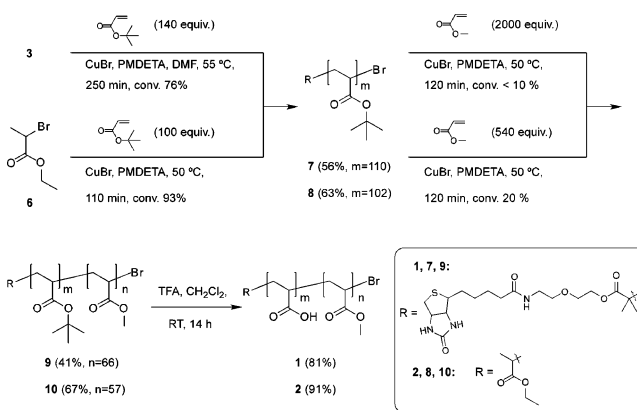
Scheme 3

Table 1. Molecular Weights and Molecular Weight Distributions for Biotinylated and Nonbiotinylated P*t*BA_m Homopolymers and P*t*BA_m-*b*-PMA_n Diblock Copolymers by ^{1}H NMR and SEC

polymer	m^a	n^a	M_n (^{1}H NMR)^b	M_n (SEC)	M_w/M_n
7	110	0	17 200	14 400	1.27
8	102	0	12 500	13 200	1.22
9	110	66	25 200	20 100	1.01
10	102	57	15 400	18 100	1.09

^{a} Number of *tert*-butyl acrylate repeating units and methyl acrylate repeating units based on SEC characterization. ^{b} Molecular weights of biotinylated polymers were determined by comparison of the integration area of the average of the protons on the biotinylated initiator at the chain end to that of the resonance of the methine groups on the polymer backbone between 2 and 2.4 ppm, in the ^{1}H NMR spectra. Molecular weights of nonbiotinylated polymers were determined by comparison of the integration area of the average of the methylene proton resonance of the ethyl ester groups and the methine group at the chain ends to that of the resonance of the methine groups on the polymer backbone between 2 and 2.4 ppm, in the ^{1}H NMR spectra.

block copolymers, **1** and **2**, was then accomplished by lyophilization (Scheme 3). The selective cleavage of the *tert*-butyl groups was demonstrated by the disappearance of the *tert*-butyl proton resonance at 1.42 ppm in the ^{1}H NMR spectra and by the disappearance of the *tert*-butyl group stretching bands at 1393 and 1367 cm⁻¹ in the IR spectra. In addition, the broadening of the carbonyl stretching band and the absorption from 3500 to 2500 cm⁻¹, characteristic of carboxylic acids, indicated the formation of PAA from P*t*BA. Although a number of solvents and solvent mixtures were employed (e.g., DMSO, THF/D₂O), upon cleavage of the *tert*-butyl groups of **9** to form amphiphilic block copolymer, **1**, the resonances for the protons of the biotin unit were no longer visible by ^{1}H NMR spectroscopy. The lack of observation of the chain end unit is consistent with a solubility behavior for a polymer having very different chain segment compositions. The primary ester linkage between the biotin unit and the polymer is stable under the TFA reaction conditions, which was confirmed by model studies whereby the biotinylated initiator treated under the same conditions for the cleavage of biotinylated PAA-*b*-PMA, **9**, was found to undergo no cleavage, as observed by ^{1}H NMR spectroscopy. Furthermore, confirmation of the persistence of the biotin chain end unit was made through assays that identified its presence on the surface of the micelles and SCK nanostructures, as described below. Glass transition temperatures T_g of **1**, **2**, and **7**–**10** were measured by differential scanning calorimetry (DSC) (Table 2).

The micellization process followed a two-step procedure. Amphiphilic block copolymer PAA-*b*-PMA was dissolved in THF (a solvent for the PMA and PAA segments), followed by

Table 2. Glass Transition Temperatures for Biotinylated and Nonbiotinylated Homopolymers and Diblock Copolymers Characterized by DSC

polymer	T_g (°C)[a] (P*t*BA)	T_g (°C)[a] (PMA)	T_g (°C)[a] (PAA)
7	45		
8	43		
9	41	not observed	
10	43	16	
1		not observed	124
2		13	123

[a] Measurements were performed with a heating rate of 10 °C/min under N_2 flow. T_g was taken as the midpoint of the inflection tangent upon the third or subsequent heating scans.

Table 3. Mixed Micelle Formation and DLS Characterization for the Mixed Micelles

micelle	biotinylated block copolymer content[a] (mol %)	amount of **1** (mg)	amount of **2** (mg)	THF amount (mL)	H_2O amount (mL)	micelle concentration (mg/mL)	D_h (nm) (number-average)
11	0%	0	60.0	60	60	0.261	26 ± 5
12	1%	0.7	58.6	60	60	0.253	27 ± 2
13	2%	1.3	58.0	60	60	0.245	28 ± 1
14	10%	6.8	62.0	64	64	0.271	29 ± 3
15	40%	12.0	18.6	30	30	0.267	32 ± 4

[a] Biotinylated block copolymer content was calculated on the basis of the molar percentage of the biotinylated PAA-*b*-PMA block copolymer to the nonbiotinylated PAA-*b*-PMA block copolymer.

the gradual addition of deionized water (a nonsolvent for PMA) into the polymer THF solution. Normally, equal volumes of water and THF were added to obtain spherical micelles with good reproducibility. The micelle stability was further established upon dialysis of the mixed H_2O/THF solution against deionized water to remove the THF solvent. The calculated concentration of the micelle solution was determined by measuring the final volume of the micelle obtained together with the initial weight of the polymer precursors used. By controlling the initial molar ratio of the biotinylated PAA-*b*-PMA to the nonbiotinylated PAA-*b*-PMA, a series of micelles and mixed polymer micelles, **11**−**15**, were formed, with a theoretical biotinylated chain incorporation of 0%, 1%, 2%, 10%, and 40%, respectively. The hydrodynamic diameters (D_h) of the micelles, **11**−**15**, were determined by dynamic light scattering (DLS) (Table 3).

Intramicellar cross-linking of the polymer micelles was achieved by intermolecular bond formation between the carboxylic acid groups in the polymer micelle shell layers, by activation with 1-[3′-(dimethylamino)propyl]-3-ethylcarbodiimide methiodide and reaction with 2,2′-(ethylenedioxy)diethylamine. Each of the micelles was cross-linked at a calculated mean-cross-linking density of 60%, based on the stoichiometry of amine functional groups of the diamino cross-linker to the carboxylic acid groups from the PAA-*b*-PMA block copolymers. The SCKs, **16**−**20**, having varying degrees of biotinylated block copolymer content, were purified by dialysis against deionized water (cellulose membrane tubing, MWCO 6000−8000 Da) to remove the unreacted cross-linker and byproducts. The amide bond formation was confirmed by IR spectroscopy with the introduction of amide I and II bands at ca. 1640 and 1560 cm^{-1}.

DLS characterization of SCKs in aqueous solution provided intensity autocorrelation functions that were deconvoluted into intensity-average hydrodynamic diameter distributions using CONTIN. The reliability of the analysis was confirmed by the
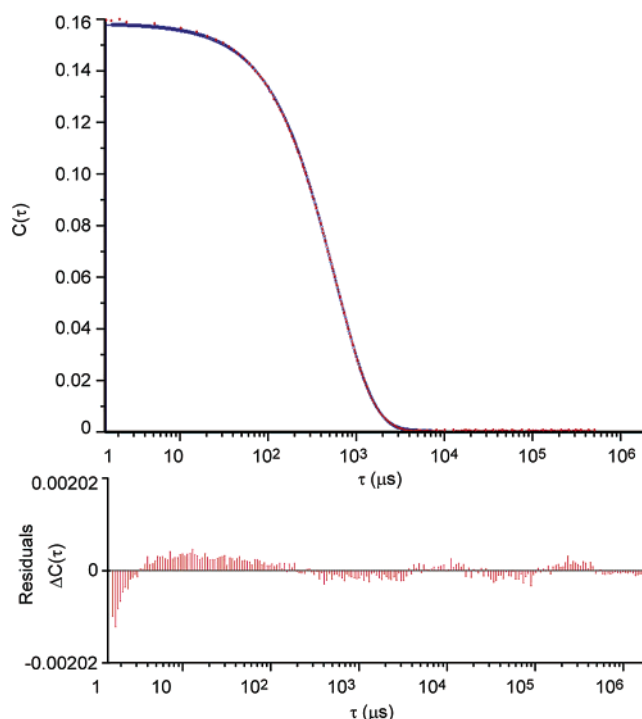
Figure 4. Intensity autocorrelation functions for the 2% biotinylated SCK, **18** (dots), and the CONTIN fit (line) at 30° scattering angle, and the residual plots for the corresponding CONTIN fit are also shown.

excellent agreement between CONTIN-computed autocorrelation functions and experimental autocorrelation functions as exemplified by the representative results shown for the 2% biotinylated SCK, **18**, in Figure 4. Small residuals found for the CONTIN analyses and depicted graphically in Figure 4 produced RMS errors on the order of 10^{-4} for all SCKs studied.

The intensity-average diameter distribution provided by CONTIN was geometrically transformed, assuming a spherical shape for the SCKs, into a volume-average diameter distribution. This was accomplished by dividing the volume fraction of nanoparticles, $V(D)$, with diameter, D, in the intensity-average diameter distribution by the product of the angular Mie scattering coefficient, $P(\theta)$, for the nanoparticle and the cube of its diameter, D^3. Under the assumption that all particles in the volume-average distribution have the same density, the volume-average distribution is equivalent to the weight-average diameter distribution.

The resulting volume-average diameter distribution was transformed into a number-average diameter distribution by dividing $V(D)$ for volume-average diameter distribution by D^3. The use of the volume- and number-average hydrodynamic diameter distributions afforded mean volume and number hydrodynamic diameters, $D_{h,volume}$ and $D_{h,number}$, respectively. The ratio, $D_{h,volume}/D_{h,number}$, served as a measure of polydispersity for the DLS-derived hydrodynamic diameter distribution that was not skewed by the minute fraction of aggregates present in aqueous solutions of the SCKs. As shown in Table 4, $D_{h,volume}/D_{h,number}$ ranged from 1.11 to 1.24 across the set of SCKs, indicating that the distributions of hydrodynamic diameter were narrow as shown in Figure 5. Measurements of hydrodynamic diameter distributions conducted at two additional angles, 30° and 125°, confirmed the finding of narrow hydrodynamic diameter distributions for all SCKs studied. In the case of micelles and SCKs prepared from 100% biotinylated PAA-*b*-

Table 4. DLS Characterization for the Biotinylated and the Nonbiotinylated SCKs

SCK[a]	biotinylated block copolymer content (mol %)	SCK concentration (mg/mL)	D_h (nm) (intensity-average)	D_h (nm) (volume-average)	D_h (nm) (number-average)	$D_{h,volume}/D_{h,number}$
16	0%	0.260	73 ± 2	31 ± 1	25 ± 2	1.24
17	1%	0.249	33 ± 3	29 ± 2	25 ± 1	1.16
18	2%	0.244	36 ± 7	31 ± 1	28 ± 1	1.11
19	10%	0.263	46 ± 1	30 ± 2	25 ± 2	1.20
20	40%	0.253	38 ± 1	30 ± 1	26 ± 1	1.15

[a] SCKs were prepared with 60% average cross-link density, as based on the ratio of amine functional groups from the diamino cross-linker to the carboxylic acid groups from the PAA-*b*-PMA block copolymer.
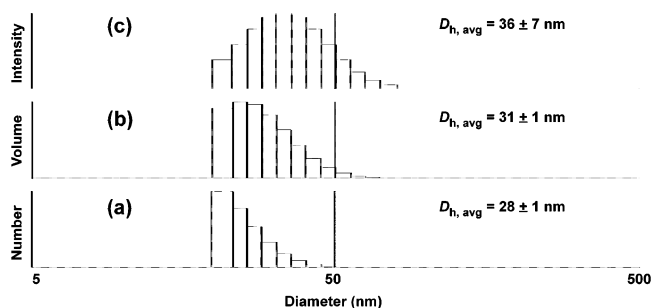
Figure 5. DLS characterization of 2% biotinylated SCK, **18**, in aqueous solution at 20 °C. Histograms are averaged by intensity, volume, and number, respectively (CONTIN fit).
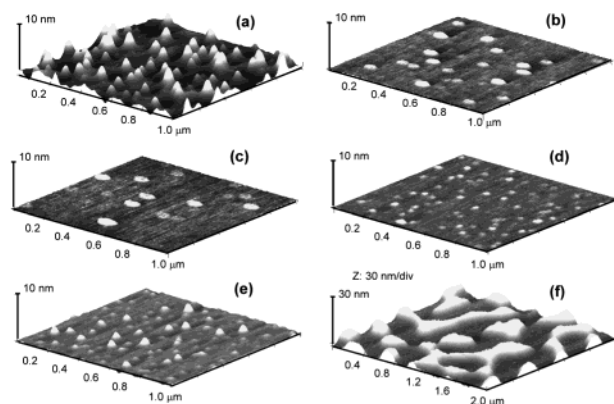
Figure 6. Tapping-mode AFM images of SCKs: (a) **16**, (b) **17**, (c) **18**, (d) **19**, (e) **20**, and (f) 100% biotinylated SCK. Samples were prepared by drop deposition onto freshly cleaved mica and allowed to dry in air.

PMA copolymers, species characterized by sizes greater than 100 nm and by nonspherical, irregular shapes were found by DLS and AFM measurements, respectively. Thus, low percentages of biotinylated block copolymer contents were chosen, ranging from 0% to 40% as mentioned above, for the study of their interactions with avidin.

The dimensions of the SCKs were characterized by tapping-mode atomic force microscopy (AFM) and transmission electron microscopy (TEM). The diameter values obtained by AFM (Figure 6) and TEM (Figure 7) were substantially larger than were the heights measured by AFM. These discrepancies are the result of the low T_g of the methyl acrylate core domain allowing for the particles to deform upon adsorption onto the solid substrates employed for AFM and TEM imaging.[74,75] In addition, the larger diameter values obtained from AFM measurements in comparison to those from TEM indicate greater deformation of the particles on the hydrophilic mica surface, the substrate for AFM characterization, as opposed to the

Table 5. Size Characterization Data for the SCKs

SCK	biotinylated block copolymer content (mol %)	$D_h{}^a$ (nm) (DLS)	$H_{av}{}^b$ (nm) (AFM)	$D_{av}{}^b$ (nm) (AFM)	$D_{av}{}^c$ (nm) (TEM)
16	0%	25 ± 2	2.6 ± 0.6	68 ± 8	30 ± 5
17	1%	25 ± 1	1.2 ± 0.5	102 ± 8	27 ± 5
18	2%	28 ± 1	1.3 ± 0.4	84 ± 11	24 ± 4
19	10%	25 ± 2	0.5 ± 0.2	65 ± 12	36 ± 7
20	40%	26 ± 1	1.0 ± 0.4	71 ± 8	26 ± 4

[a] Number-average hydrodynamic diameters of SCKs in aqueous solution were characterized by dynamic light scattering. [b] Average heights and average diameters of SCKs were measured by tapping-mode AFM, averaged from the diameters of ca. 150 particles. [c] Average diameters of SCKs were measured by TEM, averaged from the diameters of ca. 150 particles.

hydrophobic carbon surface, the substrate for TEM characterization.[75] The characterization data for the SCK samples are summarized in Table 5.

Avidin/HABA Binding Assay. The bioavailability of biotin presented from the SCKs to its protein receptor was evaluated by a competitive binding assay (avidin/HABA) and fluorescence correlation spectroscopy (FCS) studies. The amount of surface-available biotin on each functionalized SCK sample was quantified by the avidin/HABA assay.[108-111]

The results of these analyses are shown in the overlaid UV−vis spectra (Figure 8a). Upon addition of SCK nanoparticles with different biotinylated block copolymer content, the change of absorbance at 500 nm increased with an increase in biotinylated block copolymer content, suggesting the avidin/HABA complex is displaced by biotin presenting on the SCK surface. The amount of biotin in each of the biotinylated SCK sample solutions was calculated, and the data are summarized in Table 6. The amount of available biotin for each of the biotinylated SCK nanoparticles corresponded to nanomoles of biotin per milliliter of SCK sample, which increased with an increase in biotinylated block copolymer content, controlled by the initial stoichiometry of **1**:**2** during the process of mixed micelle formation.

To compare the relative amount of surface-available biotin among SCK samples, the relative amounts of biotin on the SCK surfaces were calculated by correction for concentration differences and normalization with the amount of surface-available biotin using the 1% biotinylated SCK, **17**, as the normalization standard. The normalized amount of biotin, available for interaction with avidin, for each sample is plotted against the percentage of biotinylated block copolymer content in Figure 8c. The relative numbers of biotin units exposed on the SCK surface and available for binding with avidin increased as the theoretical numbers increased.

To estimate the functional group availability obtained via the mixed micelle methodology, the amount of measured biotin based on the avidin/HABA assay was compared against the

(108) Green, N. M. *Biochem. J.* **1965**, *94*, 23c−24c.
(109) Green, N. M. *Methods Enzymol.* **1970**, *18*, 418−424.
(110) Savage, M. D. *A Laboratory Guide to Biotin-Labeling in Biomolecule Analysis*; Meier, T., Fahrenholz, F., Eds.; Birkhäuser Verlag: Basel, Boston, Berlin, 1996; pp 1−28.
(111) HABA is a dye that binds to avidin in the same binding pocket used to bind biotin. HABA has a maximum UV absorbance at 350 nm, and once an avidin/HABA complex has formed, the maximum UV absorbance shifts to 500 nm. As compared with the strong affinity for biotin exhibited by avidin ($K_d = 10^{-15}$ M), avidin's affinity for HABA is much weaker ($K_d = 10^{-6}$ M). Thus, when biotin is added to a solution of avidin/HABA complex, HABA is displaced quantitatively by biotin, and this displacement can be quantitatively monitored by the decrease in UV absorbance at 500 nm.
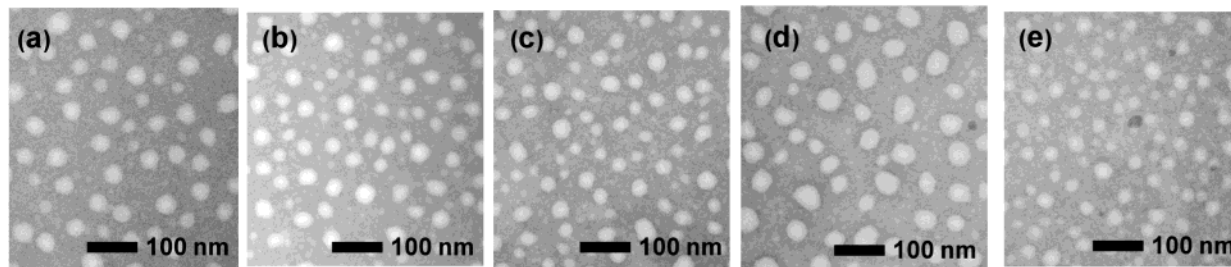
Figure 7. TEM images of SCKs: (a) **16**, (b) **17**, (c) **18**, (d) **19**, and (e) **20**. Samples were stained with phosphotungstic acid and drop deposited onto a carbon-coated copper grid.
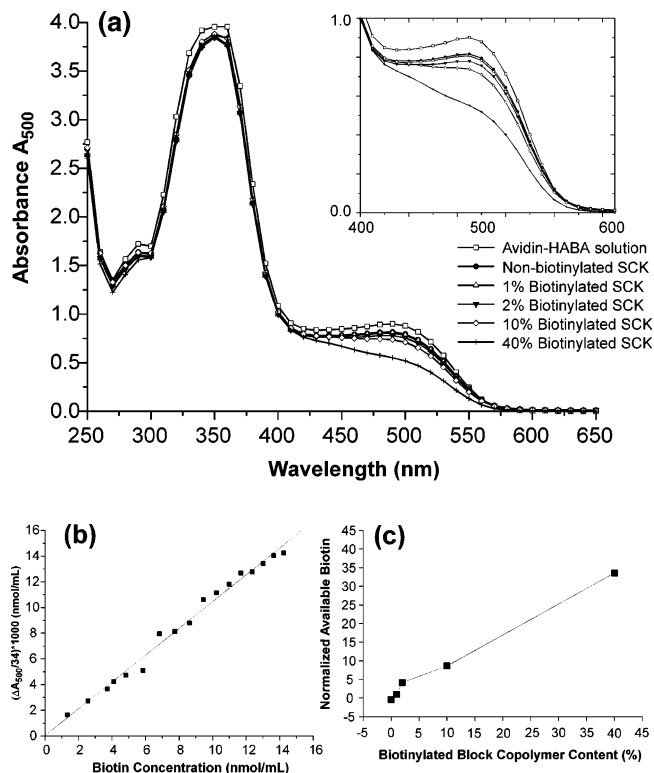

Figure 8. (a) UV−vis spectra of the avidin−HABA complex and the avidin−HABA complex added with **16**−**20**, respectively, in 50 mM PBS buffer, 50 mM NaCl, pH 7.1. The zoomed region at 500 nm is shown in the subset. (b) Calibration curve for avidin/HABA assay. (c) Normalized amount of surface-available biotin versus the biotinylated block copolymer content (**16**−**20** corresponding to 0%, 1%, 2%, 10%, and 40%, respectively).

theoretical values, which were calculated on the basis of the initial stoichiometry of **1** and **2** being used in the preparation of the mixed micelles (Table 6). The surface accessibilities of the biotin units for the micelles and SCKs were similar, as determined for the samples having 10% biotinylated block copolymer incorporation, **19**, **21**, and **22**.[112] It is uncertain whether the degree of shell cross-linking of the SCKs and rigidity of the particles play a role in the bioavailability of the surface-accessible groups. Within the experimental error, the percentage of biotin units available in comparison to those incorporated in the formulation remained consistently at 10−25%. The less than complete surface accessibility and bioavailability can be explained by several effects, although the magnitude of the contributions from each of these potential

effects is unknown. The most likely cause of reduced biotin availability was trapping of biotinylated chain ends below the nanoparticle surface during micelle formation. Other potential sources of inhibition for biotin binding include SCK cross-linking density, surface rigidity, chain dynamics, and polydispersity.

Fluorescence Correlation Spectroscopy (FCS). The multivalent binding event expected for biotinylated-SCK:protein receptor interactions was also studied using FCS. The measurement of the translational diffusion coefficient for a fluorescent species within a small focal volume is provided by FCS.[113−119] Because the diffusion of spherical molecules is inversely proportional to the cube root of the molecular weight, any association or binding interaction that leads to the increase of molecular weight will result in a decrease of the diffusion coefficient, which can be identified and quantified by the correlation time from an autocorrelation analysis of fluorescence intensity fluctuations.

The FCS instrument was home-built,[120] based on the principle of a solid immersion microscope,[121−124] and the schematic drawing of the instrumentation setup was shown in Figure 9a. Alexa Fluor 488 labeled avidin was analyzed by FCS, and a hydrodynamic diameter of 9.2 nm was found. This diameter, as expected, is small as compared with values obtained for nonfluorescence SCK nanoparticles using DLS (D_h ca. 30 nm). As a result, SCK:protein binding due to biotin−avidin recognition was expected to decrease the diffusion coefficient of the fluorescently labeled avidin. In addition, as more avidin was bound to SCK nanoparticles, a larger fraction of the slower diffusing SCK:protein complex was anticipated.

FCS measurements of Alexa Fluor 488 labeled avidin and SCKs, **16**−**20**, with different biotinylated block copolymer contents were performed in 10 mM of HEPES buffer with 1 mM EDTA, 1 M NaCl, and at pH 7.1. A high salt concentration was used to eliminate the nonspecific binding interactions.[125]

(112) Sample **21** is a 10% biotinylated micelle, prepared by mixing **1** with nonbiotinylated PAA$_{93}$-*b*-PMA$_{76}$, M_n^{SEC} = 18 600 g/mol, M_w/M_n = 1.12, which is slightly different from the nonbiotinylated block copolymer, **2**, used to prepare **19**, and sample **22** is the corresponding SCK prepared from **21**, with 60% cross-linking density.

(113) Elson, E. L.; Magde, D. *Biopolymers* **1974**, *13*, 1−27.
(114) Magde, D.; Elson, E. L.; Webb, W. W. *Biopolymers* **1974**, *13*, 29−61.
(115) Schwille, P.; Oehlenschläger, F.; Walter, N. G. *Biochemistry* **1996**, *35*, 10182−10193.
(116) Wohland, T.; Friedrich, K.; Hovius, R.; Vogel, H. *Biochemistry* **1999**, *38*, 8671−8681.
(117) Schüler, J.; Frank, J.; Trier, U.; Schäfer-Korting, M.; Saenger, W. *Biochemistry* **1999**, *38*, 8402−8408.
(118) Medina, M. Á.; Schwille, P. *BioEssays* **2002**, *24*, 758−764.
(119) Haustein, E.; Schwille, P. *Methods* **2003**, *29*, 153−166.
(120) Clark, C. G., Jr.; Remsen, E. E.; Wooley, K. L., manuscript in preparation.
(121) Mansfield, S. M.; Kino, G. S. *Appl. Phys. Lett.* **1990**, *57*, 2615−2616.
(122) Ghislain, L. P.; Elings, V. B. *Appl. Phys. Lett.* **1998**, *72*, 2779−2781.
(123) Ghislain, L. P.; Elings, V. B.; Crozier, K. B.; Manalis, S. R.; Minne, S. C.; Wilder, K.; Kino, G. S.; Quate, C. F. *Appl. Phys. Lett.* **1999**, *74*, 501−503.
(124) Koyama, K.; Yoshita, M.; Baba, M.; Suemoto, T.; Akiyama, H. *Appl. Phys. Lett.* **1999**, *75*, 1667−1669.
(125) Swamy, M. J.; Marsh, D. *Biochemistry* **2001**, *40*, 14869−14877.

Table 6. Results of the Avidin/HABA Assay for the Micelle and SCK Samples

sample	biotinylated block copolymer content (mol %)	sample concentration[a] (mg/mL)	theoretical value of available biotin[b] (nmol/g)	$(\Delta A_{500}/34)$ $\times 1000^c$ (nmol/mL)	available biotin per milliliter of sample solution[d] (nmol/mL)	available biotin per gram of polymer[e] (nmol/g)	fraction of surface-available biotin[f]
16	0%	2.53	0	0	0	0	n/a
17	1%	2.59	900	0.3	0.3	99	11%
18	2%	1.39	1680	0.7	0.6	410	25%
19	10%	2.93	7560	2.7	2.5	850	11%
21	10%	2.63	7520	4.3	4.1	1600	22%
22	10%	2.51	7520	3.7	3.4	1400	19%
20	40%	2.45	30 000	8.2	8.1	3300	11%
15	40%	1.38	30 000	5.0	4.8	3500	12%

[a] The micelle and SCK samples were concentrated using a stirred ultrafiltration cell equipped with an ultrafiltration membrane filter disk (NMWL 100 000 Da). [b] Theoretical values of the surface-available biotins based on the initial molar ratios of the biotinylated PAA-*b*-PMA to the nonbiotinylated PAA-*b*-PMA during the preparation; the data are represented in units of nanomoles of biotin per gram of polymer precursor mixture. [c] $(\Delta A_{500}/34) \times 1000$ was used to calculate the amount of biotin in the sample solution being analyzed in nmol/mL. [d] Surface-available biotin in the SCK or micelle solution by comparison of the absorbance change with that of the calibration curve. [e] Surface-available biotin per gram of polymer precursor mixture based on the calculated concentration of the sample solutions used in each assay. [f] Fraction of the surface-available biotin is the molar percentage of available biotin to the theoretical value.
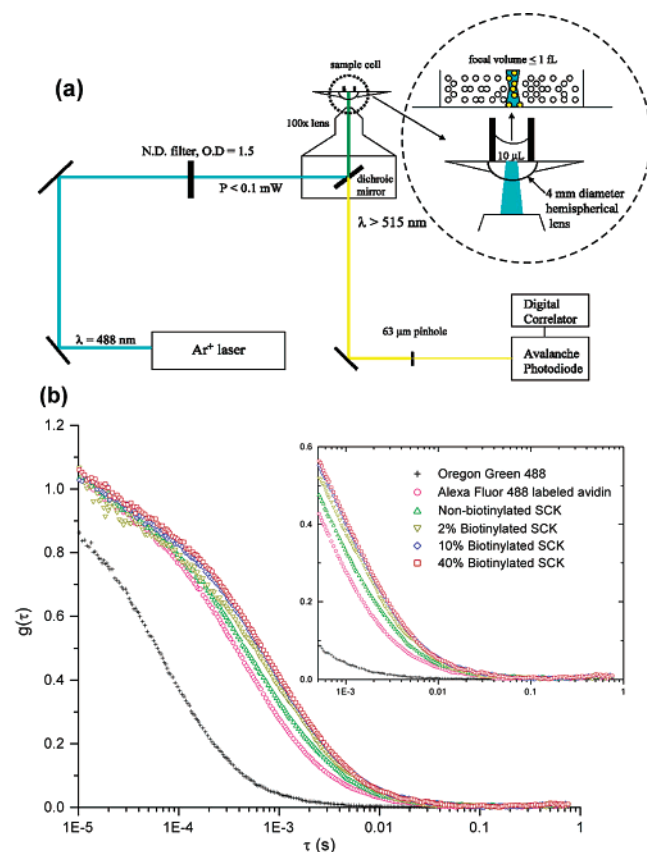

Figure 9. (a) Schematic drawing of FCS instrumentation setup; (b) normalized autocorrelation function of Oregon Green 488, Alexa Fluor 488 conjugate, and mixture of Alexa Fluor 488 conjugate with **16**−**20**, in 10 mM HEPES buffer with 1 mM EDTA and 1 M NaCl, pH 7.1, respectively. A zoomed region of the autocorrelation function is shown in the subset.

The same concentration of the labeled avidin used to characterize the diffusion coefficient for a solution of pure labeled protein was employed for each SCK:protein solution mixture. Normalized fluorescence intensity autocorrelation functions for SCK: protein mixtures, the pure labeled protein, and an Oregon Green 488 calibration standard are shown in Figure 9b.

The correlation time τ_d for each measurement was calculated by fitting the autocorrelation function. To calculate the diffusion coefficient of the samples, Oregon Green 488 was used to characterize the focal volume. The correlation time was converted to diffusion coefficient by reference to the τ_d of

Table 7. Data Summary for the FCS Measurement

	N	$\tau_d \times 10^{-5}$ (s)	$D_T \times 10^{-11}$ (m² s⁻¹)	$D_h{}^c$ (nm)	$D_h{}^d$ (nm)	$X_{bound}{}^e$
OG[a]	8.2	6.4 ± 0.7	27 ± 3	1.5 ± 0.2		
avidin[a]	0.67	41.7 ± 0.5	4.1 ± 0.6	9.2 ± 1.4		
16	0.72	50.5 ± 0.6	3.4 ± 0.5	11.2 ± 1.7	31 ± 1	0.14
18	0.76	62.1 ± 0.9	2.8 ± 0.4	13.8 ± 2.2	31 ± 1	0.32
19	0.87	65.1 ± 1.0	2.6 ± 0.4	14.4 ± 2.2	30 ± 2	0.42
20	0.79	73.0 ± 1.0	2.4 ± 0.4	16.2 ± 2.6	30 ± 1	0.41
20[b]	17	78.4 ± 0.6	2.2 ± 0.3	17.4 ± 2.7	30 ± 1	0.47

[a] OG is Oregon Green 488; avidin is Alexa Fluor 488 labeled avidin. [b] The same 40% biotinylated SCK sample, with a 10-fold increase of the avidin concentration. [c] Hydrodynamic diameters of the fluorescent species calculated from correlation time τ_d. [d] Volume-average hydrodynamic diameters of SCKs from DLS measurements, which were used to calculate τ_{bound} for the fitting into the two-component model, eq 5 in the Supporting Information. [e] Fraction of avidin−SCK complex, calculated by fitting with eq 5 (Supporting Information).

Oregon Green 488, whose diffusion coefficient was determined via calibration with Rhodamine 6G having a known diffusion coefficient of 2.80×10^{-10} m² s⁻¹ (at 22 °C).[126] Correlation times and diffusion coefficients are summarized in Table 7. The correlation time τ_d increased as the biotinylated block copolymer content in each SCK sample increased, indicating more labeled avidin was bound to SCK per unit concentration of avidin in the solution, which additionally suggested that more biotin was available to its protein receptors. The averaged hydrodynamic diameters of the fluorescent species in each solution were calculated using eqs 3 and 4 (Supporting Information), by employing Oregon Green 488 as a calibrant for the calculation of D_T. The fluorescent species in solution were also analyzed as either free labeled avidin or labeled avidin-bound SCKs using a two-component model, eq 5 (Supporting Information). The calculation of diffusion coefficients and the averaged hydrodynamic diameters of the fluorescent species using Oregon Green 488 as calibrant have an experimental error up to 16% in each determination, which mainly arise from the determination of the correlation time of Oregon Green 488. However, the correlation time determination for each sample is independent of the calibrant, so the trend observed in the determination is valid. The calculations for the bound fraction of the fluorescent species using the two-component model are also not affected.

(126) Rigler, R.; Mets, Ü.; Widengren, J.; Kask, P. *Eur. Biophys. J.* **1993**, *22*, 169−175.

In agreement with the avidin/HABA assay, these FCS measurements found that the amount of available biotin at the surface of the biotinylated SCK nanoparticles increased with increasing biotin-terminated block copolymer incorporation, as evidenced by the increasing correlation times, and the fraction of biotin that underwent binding with avidin was ca. constant. To confirm there was no significant amount of available biotin that remained unbound, the 40% biotinylated SCK sample was also analyzed with an avidin concentration increased by 10-fold. Under conditions of excess avidin, the lack of a significant change of the hydrodynamic diameter of the avidin−SCK complex and the presence of free avidin indicated a saturation of the biotinylated SCKs with labeled avidin.

Conclusions

A novel biotinylated initiator was synthesized and utilized to initiate, via ATRP, homo- and diblock copolymer bearing a single biotin moiety at the chain terminus. The chain terminal biotinylated amphiphilic diblock copolymer PAA-*b*-PMA was mixed in solution with its nonbiotinylated analogue to form mixed micelles. The mixed micelle approach offers control over the functional group incorporation within the nanoparticles by varying the stoichiometric ratio of the functionalized to non-functionalized micelle precursors. Intramicellar cross-linking within the PAA shell layer converted the supramolecular assemblies to robust SCK nanoparticles presenting bioactive biotin.

The surface- and bioavailability of the biotinylated SCK nanoparticles, comprised of different percentages of biotinylated block copolymer, were evaluated using an avidin/HABA competitive binding assay and FCS. Data from these studies support the trend that greater numbers of biotin were available to bind with the protein receptors with an increase in the biotinylated block copolymer incorporation. It is important to note that the shell cross-linking of the nanostructure presenting the biotin did not diminish the bioavailability for binding with the biological macromolecules. The avidin/HABA assay quanti-fied the amount of available biotin to be less than 25% of the theoretical value, likely due to the loss of functional group availability in the process of micellization and shell cross-linking. However, kinetic studies that remain in progress are revealing that the binding interactions are significantly more complex than is considered here. These preliminary studies indicate that there are kinetic differences and differences in the ultimate level of available biotin units observed between the samples; the rates of binding increase and the percentage of available biotin units decrease with increasing biotinylation. FCS results indicated the same trend for the binding capacity of 10% and 40% biotinylated SCKs. With the enhanced sensitivity of fluorescence cross-correlation spectroscopy,[118] the binding isotherm of the biotinylated SCKs of different biotin surface coverage might be determined accurately, potentially advancing the understanding of the thermodynamics and kinetics of this multivalent model system. Geometric considerations, involving hard sphere surface contacts, indicate that approximately 60 avidins[127] can be accommodated through binding upon the surface of an SCK having a hydrodynamic diameter of 30 nm
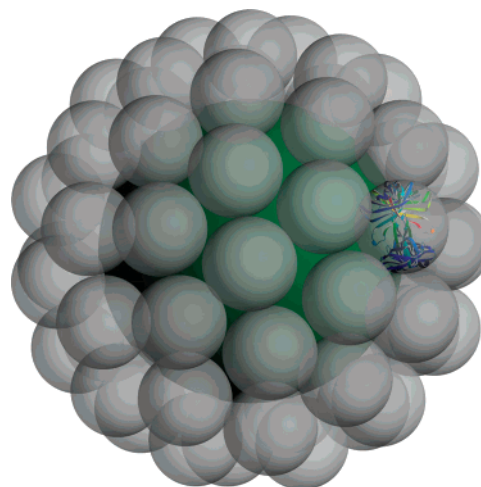

Figure 10. Schematic illustration of 60 avidins (with a diameter of 9.2 nm) packing at the surface of SCK (with a diameter of 30 nm) based on "hard sphere" surface contacts.

(Figure 10). Accurate values of the SCK aggregation numbers are yet to be determined, but they can be estimated to be between 400 and 800 when comprised from the diblock copolymers of ca. 13 000 Da, which suggests that there will be significant steric effects that will prevent the binding of avidins to all of the biotin units present.

These early findings are instructive, indicating that binding of biological macromolecules to the SCKs functionalized with bioactive moieties is a complex process that can be controlled, but which also requires substantial further investigation to be understood. These initial results demonstrate a mechanism for the preparation of well-defined nanostructured materials that serve as a model for the study of molecular ligands, immobilized on a nanoscopic surface, and recognized by their protein receptors, a pervasive phenomenon in biological systems. Further studies are in progress, utilizing the control in the preparation of biotinylated SCK nanoparticles, and in conjunc-tion with the compositional versatility and structural stability of SCK nanoparticles as robust nanoscopic building blocks to form supramolecular assemblies, namely fabrication of 2-D and 3-D nanostructured materials with biotinylated SCKs employing biotin−avidin recognition.

Supporting Information Available: Full experimental details and characterization data. This material is available free of charge via the Internet at http://pubs.acs.org.

JA039647K

(127) Using the angle (27.15°) between by two adjacent circles of radius 4.6 on the surface of a circle radius 15, the maximum number of smaller spheres that can be packed on the surface of the larger sphere is 60. Sloane, N. J. A.; Hardin, R. H.; Smith, W. D., and others. Spherical Codes. http://www.research.att.com/∼njas/packings/index.html (accessed October 2003).